Solution Structure of Cryptdin-4, a Mouse Paneth Cell α-Defensin[†,‡]

Weiguo Jing,[§,||] Howard N. Hunter,[§,||] Hiroki Tanabe,[⊥] Andre J. Ouellette,[⊥] and Hans J. Vogel*[,§]

Structural Biological Research Group, Department of Biological Sciences, University of Calgary, Calgary, Alberta T2N 1N4, Canada, and Departments of Pathology and Microbiology and Molecular Genetics, College of Medicine, University of California, Irvine, California 92697-4800

Received June 29, 2004; Revised Manuscript Received September 24, 2004

ABSTRACT: Mammalian defensins are abundant antimicrobial peptides that contribute to host defense. They are characterized by several conserved amino acids, including six invariant cysteine residues which form three intramolecular disulfide bonds and stabilize the tertiary structure. Cryptdin-4 (Crp4), a mouse α-defensin with potent *in vitro* bactericidal activity, has a primary structure distinct from all known α-defensins in that its polypeptide backbone uniquely lacks three residues between Cys^{IV} and Cys^{V}. NMR diffusion experiments showed that Crp4 is monomeric in solution, and its three-dimensional solution structure, determined by two-dimensional proton NMR, consists of a triple-stranded antiparallel β-sheet with the β-strands joined to each other by a series of tight turns and a β-hairpin. However, the overall β-sheet content in Crp4 is lower than that of other α-defensin structures, while the shape and orientation of the Crp4 β-hairpin also differ from those of other α-defensin structures. These structural characteristics combined with the high overall cationicity of Crp4 may contribute to its broad bactericidal spectrum and membrane disruptive activity.

The gene-encoded mammalian defensins, a family of small cationic proteins, are characterized by six cysteine residues that form three intramolecular disulfide bonds. On the basis of amino acid sequence similarities and the connectivities of the six cysteine residues, defensins may be classified into three subfamilies: α-, β-, and θ-defensins (*1*). As a class of antimicrobial peptides (AMPs),[1] defensins exhibit broad microbicidal activity against Gram-positive and Gram-negative bacteria, yeast, fungi, mycobacteria, spirochetes, and enveloped viruses (*1*, *2*). In addition, some defensins have been reported to be able to act as chemokines, activating the adaptive immune response (*3*−*5*). At present, mammalian defensins are among the most intensely studied AMPs.

The mammalian α-defensins are 29−35 residues in length, with specific Cys^{I}−Cys^{VI}, Cys^{II}−Cys^{IV}, and Cys^{III}−Cys^{V} disulfide connectivities. They were first isolated from myeloid cells (*6*) and later identified in intestinal Paneth cells (*7*), and α-defensins RK-1 and RK-2 were found in rabbit kidney (*8*, *9*). So far, six α-defensins have been isolated from humans; four of them (HNP-1−HNP-4) are stored in azurophilic granules of the neutrophil, and two (HD-5 and HD-6) occur in secretory granules of the Paneth cells (*10*). Enteric α-defensins are released by Paneth cells from the base of the crypts of Lieberkühn in the small intestine as components of apically oriented granules. The secretory granules are discharged in response to cholinergic stimulation or exposure to bacteria or bacterial antigens (*11*−*13*), and they contain varied AMPs and proteins (*14*), including lysozyme (*15*−*17*), secretory phospholipase A_2 (18), angiogenin-4 (*19*), and α-defensins, termed cryptdins (Crps) in mice (*20*−*22*). In *in vitro* assays, Crp4 is the most potent of the known mouse α-defensin peptides (*23*).

Paneth cell α-defensins confer enteric immunity (*3*), and thus, knowledge of determinants of peptide activity and biosynthesis will improve the understanding of their role in mucosal immunity. For example, cryptdins (Crps) are secreted into the lumen of small intestinal crypts at concentrations of 25−100 mg/mL, 4 orders of magnitude greater than their *in vitro* minimum bactericidal concentrations (*4*). In mice, Paneth cell α-defensin precursors (proCrps) are processed to their biologically active forms by specific proteolytic cleavage events catalyzed by matrix metalloproteinase-7 (MMP-7, matrilysin). Disruption of the MMP-7 gene abrogates proCrp activation, eliminating the accumulation of functional mature Crp peptides from the small intestine (*5*). Consequently, MMP-7-null mice have impaired enteric innate immunity in response to oral bacterial infections (*5*). Also, in mice transgenic for the human Paneth cell α-defensin HD5, the minitransgene is expressed specifically in Paneth cells, and the mice are immune to oral infection by virulent strains of *Salmonella enterica* serovar Typhimurium (*3*).

In this study, we have determined the three-dimensional solution structure of Crp4 by two-dimensional ^{1}H NMR to

[†] This work was supported by an operating grant from the Canadian Institute of Health Research to H.J.V. and NIH Grant DK44632 to A.J.O. H.J.V. and W.J. hold senior scientist and postdoctoral fellowship awards, respectively, from the Alberta Heritage Foundation for Medical Research (AHFMR).

[‡] The atomic coordinates and structure factors (entry 1TV0) have been deposited in the Protein Data Bank.

* To whom correspondence should be addressed. Phone: (403) 220-6006. Fax: (403) 289-9311. E-mail: vogel@ucalgary.ca.

[§] University of Calgary.

[||] These authors contributed equally to this work.

[⊥] University of California.

[1] Abbreviations: Crp4, cryptdin-4; AMPs, antimicrobial peptides; TOCSY, total correlation spectroscopy; NOE, nuclear Overhauser effect; NOESY, NOE spectroscopy; DQF-COSY, double-quantum-filtered correlation spectroscopy; CSI, chemical shift index.

10.1021/bi048645p CCC: $27.50
Published on Web 11/23/2004

FIGURE 1: Amino acid sequences of mouse cryptdins (Crp1−5) and the α-defensins from rabbit kidney RK-1 and human neutrophil HNP-3. The six conserved cysteine residues are highlighted.

improve our understanding of structure−function relationships in the peptide and to gain insight into how this structurally unique α-defensin contributes to innate immunity. To date, the three-dimensional structures of a number of α-defensins have been determined by both NMR and X-ray crystallography techniques (partially reviewed in ref *24*). The reported three-dimensional structures for α-defensins contain a triple-stranded antiparallel β-sheet motif, a criterion for identifying peptides as α-defensins. Generally, the factors that modulate the antimicrobial spectrum and activity of α-defensins remain largely unexplained. Studies of Crp4 structure−activity relationships have shown that paired charge reversal mutations at Arg residues in the Crp4 peptide result in the loss of function in bactericidal activity and peptide−membrane interactions, suggesting that the net positive charges are important determinants of Crp4 bactericidal activity (*25*). Unlike nearly every known α-defensin in which nine amino acids separate the fourth and fifth cysteine residues, the Crp4 primary structure lacks three amino acid residues between these two cysteines (Figure 1), and we tested the hypothesis that this divergence from the α-defensin consensus primary structure affects Crp4 tertiary structure. In particular, we predicted that the hairpin loop connecting the β2 and β3 strands could diverge from the consensus and, in turn, modulate the function of this unique defensin.

MATERIALS AND METHODS

Preparation of the Recombinant Crp4 Peptide. Recombinant Crp4 was expressed in *Escherichia coli* as an N-terminal His_6-tagged fusion protein (*26*) and purified to homogeneity by reverse-phase high-performance liquid chromatography (RP-HPLC) after chemical cleavage with CNBr and verified by analytical RP-HPLC and polyacrylamide electrophoresis. The molecular mass of Crp4 was determined by MALDI-TOF MS, and the antimicrobial activity was tested as described previously (*26*).

NMR Spectroscopy. The NMR sample of Crp4 was prepared by dissolving approximately 3.2 mg of peptide in 500 μL of a 9:1 H_2O/D_2O mixture and adjusting the pH to ~4.2 using dilute HCl or NaOH. Sodium 2,2-dimethyl-2-silapentane-5-sulfonate (DSS) was added as an internal chemical shift reference compound (0 ppm).

Proton NMR experiments were performed on Bruker Avance 700 and 500 MHz spectrometers, equipped with a triple-resonance probe and a cryoprobe, respectively. To determine the optimal NMR conditions for Crp4, preliminary two-dimensional TOCSY (mixing time of 120 ms) (*27*) and NOESY (mixing time of 250 ms) (*28*) NMR spectra were acquired on the Bruker Avance 500 MHz spectrometer at 25, 30, and 35 °C. The 30 °C spectrum gave the optimum balance between line width and chemical shift distribution; therefore, this temperature was used for the detailed two-dimensional (2D) NMR data collection on the Bruker Avance 700 MHz spectrometer. DQF-COSY (*29*), TOCSY (with a mixing time of 120 ms), and NOESY (with mixing times of 200, 300, and 400 ms) spectra were acquired. Water suppression was achieved using the excitation sculpting technique (*30*) in both NOESY and TOCSY experiments. In the DQF-COSY experiment, the water signal was suppressed using the 3-9-19 Watergate pulse sequence with gradients and presaturation during the relaxation delay. All 2D data were collected with 2048 and 600 data points in the F_2 and F_1 dimensions, respectively, using spectral widths of 6500 Hz. To determine which amides were in slow exchange with the solvent, the Crp4 NMR sample was lyophilized and redissolved in 99.9% D_2O. Immediately after this, a one-dimensional ^1H spectrum was acquired followed by a series of one- and two-dimensional ^1H spectra over the following 24 h.

All 2D data were processed with NMRPipe version 3.4 (*31*) and analyzed with the NMRView version 4.1.3 (*32*) software package on workstations operating with RedHat version 7.1 of the Linux operating system. The data were zero-filled in each dimension and Fourier-transformed with a shifted sine-bell squared function.

NMR Diffusion Experiment. To determine the aggregation state of Crp4 at the concentration used for NMR experiments, a diffusion experiment was performed at 700 MHz using dioxane as an internal standard (*33*). Approximately 2.5 μL of a 1% solution of dioxane in D_2O was added to the Crp4 NMR sample in D_2O. Pulsed field gradient diffusion experiments were collected with the PG-SLED sequence (*34*, *35*). Using the Bruker XWINNMR software package, the decay of the peak intensity as a function of gradient strength was used to determine the relative diffusion constants.

Structure Calculation. The assignment of proton chemical shifts was performed using the standard methodology developed by Wüthrich (*36*). Spin systems were identified in the TOCSY spectrum, and sequential assignments were made by observing $H^{\alpha}(i)-H^{N}(i+1)$ cross-peaks in the NOESY spectrum. Upon completion of the proton assignments, NOE-based distance restraints were obtained from the NOESY spectra on the basis of NOE peak intensities using NMRView. The ϕ dihedral angles were constrained by the addition of Karplus coupling constant constraints when the coupling constants measured from the DQF-COSY spectrum exceeded 8 Hz. Additionally, broad dihedral angle restraints (between −35° and −180°) were used to confine the bond angles for the non-Gly and -Pro residues, where a coupling constant could not be easily determined. Initial structures were generated from restraints of unambiguous NOEs and dihedral angles, and then disulfide bond restraints were incorporated into the structure calculations. Protein structures were calculated using ARIA version 1.2 (*37*). ARIA enables the incorporation of ambiguous NOE distance restraints into structure calculation as well as calibration of the NOE distance restraints using a structure-based NOE back-calculation. ARIA runs were performed using the default parameters supplied in the program. Hydrogen bond restraints were added to the final calculation. Of the 100 resulting structures, the 20 lowest-energy structures were kept. Structures were analyzed with MOLMOL (*38*) and GRASP (*39*).

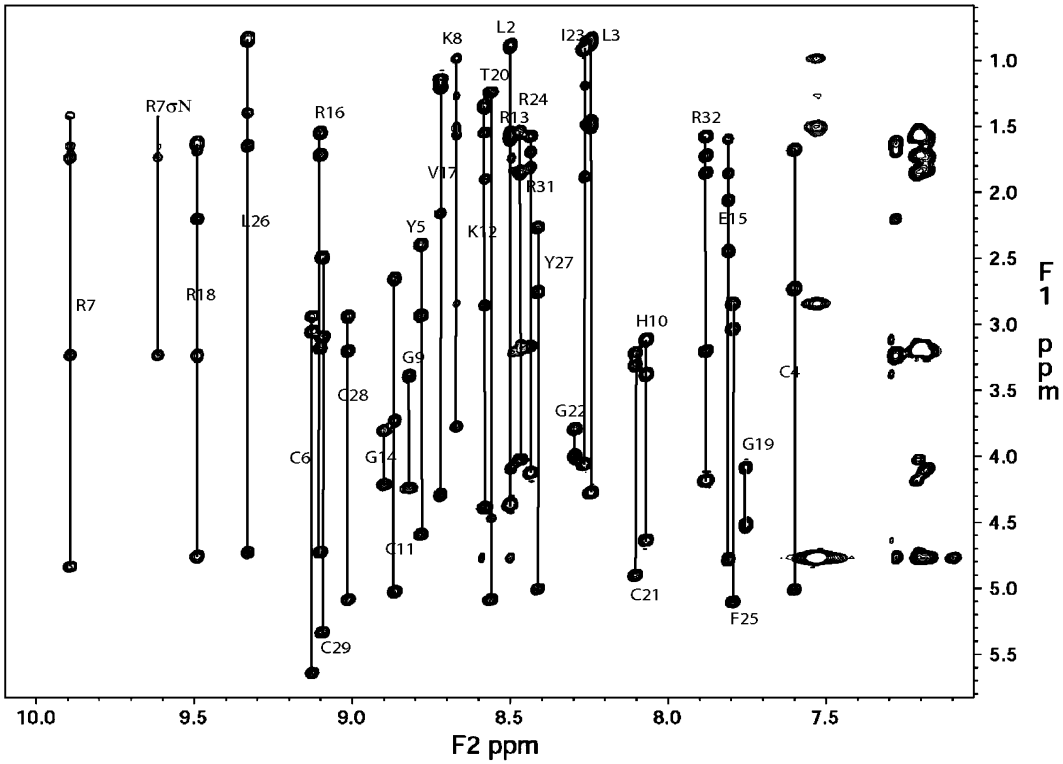

FIGURE 2: Fingerprint region of the 2D TOCSY spectrum of Crp4 acquired at 30 °C and pH 4.2. Individual amino acid spin systems are denoted with vertical lines.

RESULTS

Using an empirical equation (*40*), the calculated hydrodynamic radius of Crp4 was estimated to be 12.98 Å while the experimental value obtained from NMR diffusion is 12.64 Å. Since the calculated hydrodynamic radius of a dimer is 15.87 Å, the experimental value indicates that Crp4 is a monomer at the concentration used for structure determination. This method has been used successfully to study the aggregation properties of AMPs and small proteins (*41*−*43*). Peptides prone to dimerization or aggregation show increased measured values of the hydrodynamic radius (*42*).

The 2D NMR spectra of Crp4 acquired at 30 °C demonstrated very good chemical shift dispersion. Using the standard method, a near-complete proton assignment was obtained. Spectra obtained at 25 and 35 °C were helpful in resolving several overlapping peaks and in confirming all resonance assignments. Figure 2 shows the fingerprint region of the TOCSY spectrum acquired at 30 °C with each amino acid highlighted. An interesting observation in this TOCSY spectrum was that the chemical shift of the side chain NH proton of Arg7 (9.68 ppm) was shifted significantly downfield from the expected value (7.30 ppm) (*36*). Such a shift is most likely due to deshielding brought on by diamagnetic anisotropy from a polar group or aromatic ring. Coincidently, the 2D NOESY experiment indicated the presence of a proton signal attributed to the four terminal NH protons from Arg7. Normally, these protons are not observed in either the TOCSY or NOESY spectra due to fast exchange with solvent. It is possible that the imidazole ring from His10 coordinates to the charged side chain of Arg7. Proton exchange between the two side chains could be sufficiently slow to be viewed on the NMR time scale. Pro30 was demonstrated to be in the trans conformation based on the $d_{\alpha\delta}(i-1,i)$ NOE between the Pro and the preceding Cys29.

Crp4 is known to contain six disulfide-linked cysteines; however, it is often difficult to unambiguously determine the cysteine linkages by chemical methods. During the first run of the ARIA calculation, no disulfide bond restraints were included. However, many inter-cysteine NOEs that usually characterize a disulfide bond, such as Hα of Cys6 and Hβ of Cys21, Hα of Cys29 and Hα of Cys4, Hα of Cys29 and Hβ of Cys4, Hβ of Cys11 and Hβ of Cys28, Hβ of Cys6 and Hβ of Cys28, and Hβ of Cys6 and Hβ of Cys21, were observed in the NOESY spectrum, and these NOEs are consistent with their peak intensities, suggesting that the known disulfide bond pattern for the other α-defensins, i.e., Cys^{I}−Cys^{VI}, Cys^{II}−Cys^{IV}, and Cys^{III}-Cys^{V}, is also correct for the recombinant Crp4. This disulfide bonding pattern was incorporated in all the latter ARIA runs. Additionally, to ensure that these NOEs were not due to structural packing, we also used different disulfide bonding patterns, but such calculations gave rise to more NOE violations and structures with energies much higher than the consensus α-defensin disulfide connectivities.

As shown in Figure 3, the short- and medium-range NOEs and the chemical shift index (CSIs) (*44*) indicated that the secondary structure of Crp4 may be composed of three β-strands located in the sequence of residues 5−7, 15−21, and 25−29. This β-sheet structure was further supported by the data obtained from the D_2O exchange experiment. More than 24 h after Crp4 was redissolved in D_2O, seven of the 30 backbone NH correlations were still visible in the 2D TOCSY experiment. These belonged to Tyr5, Arg7, Arg16, Leu26, Tyr27, Cys28, and Cys29. All these slowly exchanging amides corresponded to the β-strand region established by the CSI, indicating that they should be constrained in the hydrogen bonds between the strands. These amide protons were ascribed to the hydrogen bond donors. The assignment

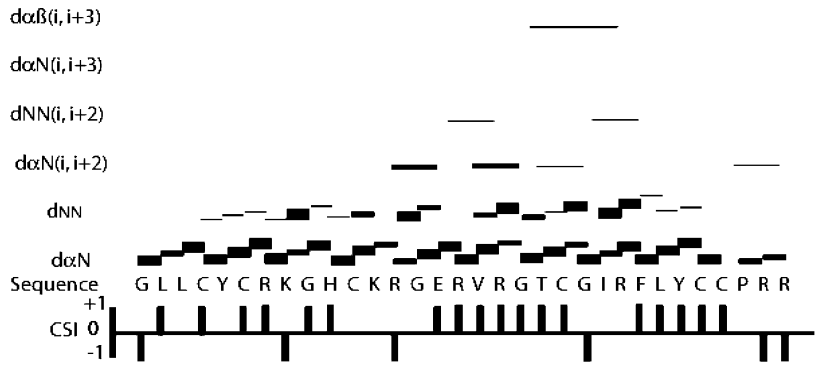

FIGURE 3: Summary of interresidue NOE connectivities for Crp4. The strong, medium, and weak NOEs are indicated by variations in the relative intensity of each of the lines. The chemical shift index (CSI) of the Hα backbone atoms is also presented.

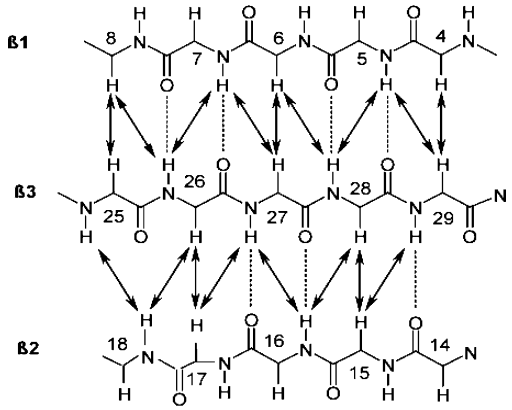

FIGURE 4: Interresidue NOEs and hydrogen bonds observed between the three separate β-strands. Dotted lines represent hydrogen bonds, and arrows with solid lines represent NOEs.

of hydrogen bonds along with the corresponding NOEs is presented in Figure 4.

Solution NMR Structure of Crp4. Altogether, 635 NOE-based distance restraints were used to calculate the structure of Crp4, including 278 interresidue, 146 sequential, 52 medium-range, and 159 long-range distance restraints. Hydrogen bonds were introduced into the structure calculation only after amide proton and carbonyl oxygen distances were within 2.4 Å and the plane of the bond did not exceed 35°, as determined by MOLMOL. The final 20 lowest-energy structures all have NOE violations of <0.5 Å and dihedral violations of <1.5°. They overlay with a global rms deviation of 0.46 Å for the backbone atoms and 1.503 Å for the heavy atoms of residues 3−30. The statistical data summarizing the quality of these 20 structures are presented in Table 1.

Crp4 possesses a small three-stranded antiparallel β-sheet structure (Figure 5). Strands β1−β3 are formed by residues 5−7, 15−18, and 25−28, respectively. The amide protons of Tyr5 and Arg7 in strand β1 form hydrogen bonds with the carbonyl oxygens of Leu26 and Cys28 in strand β3. Strand β1 is connected with strand β2 by a type IV turn for residues 8−10 and a type I turn for residues 11−14. The second turn is stabilized by a disulfide bond between Cys11 and Cys28. Strand β2 follows this turn and is connected with strand β3 by a β-hairpin consisting of two type I turns, from residues 18−21 and 22−25. The N- and C-termini of Crp4 are in the proximity of each other due to the disulfide bond formed by Cys4 and Cys29.

Closer inspection of the proton NOEs indicated that two distinct conformations could exist for the unstructured region between Gly9 and Gly14. This would seem to be reasonable due to the presence of glycine residues near both turns of this section. The presence of glycines may result in flexibility giving rise to multiple conformations in this region. Similar conformational flexibility caused by the presence of a proline residue was found in RK-1 (*45*). In addition, there are some interactions in the NOESY spectrum between residues 17−19 and 20−27. However, the β2 strand cannot make a regular β-strand in the section of residues 17 and 18 because the side chains of these residues would stick directly into the side chains from residues 26 and 27. The β2 strand contains a β-bulge caused by these steric interactions of the bulky side chains of Val17 and Arg18, minimizing their interactions with Leu26 and Tyr27. A similar β-bulge has been found in the previously determined structures of mammalian defensins.

Electrostatic Surface Properties of Crp4. Crp4 exhibited an amphipathic structure with the hydrophobic residues forming two hydrophobic faces with positively charged

Table 1: Summary of Structural Statistics for Crp4

no. of distance restraints	
interresidual	278
sequential	146
medium-range	52
long-range	159
unambiguous NOEs	607
ambiguous NOEs	28
unassigned NOEs	0
total NOEs	635
no. of broad dihedral restraints	26
rms distances from ideal values	
bonds (Å)	$3.89 \times 10^{-3} \pm 1.54 \times 10^{-4}$
angles (deg)	$(0.504 \pm 2.50) \times 10^{-2}$
impropers (deg)	1.30 ± 0.134
van der Waals (kcal/mol)	23.10 ± 2.56
distance restraints	
unambiguous (Å)	$(7.42 \pm 1.47) \times 10^{-2}$
ambiguous (Å)	$(1.71 \pm 1.46) \times 10^{-2}$
all distance restraints (Å)	$(7.16 \pm 1.41) \times 10^{-2}$
dihedral restraints (deg)	$3.09 \times 10^{-3} \pm 1.31 \times 10^{-2}$
nonbonded energies	
electronic (kcal/mol)	-836.49 ± 49.98
van der Waals (kcal/mol)	-238.26 ± 5.07
Ramachandran (%)[a]	
most favored	72.0
additionally allowed	28.0
generously allowed	0.0
disallowed	0.0
global rms distance (Å)[b]	
backbone (residues 3−30)	0.459
heavy atoms (residues 3−30)	1.503

[a] As determined by PROCHECK (*55*). [b] Calculated using MOLMOL.

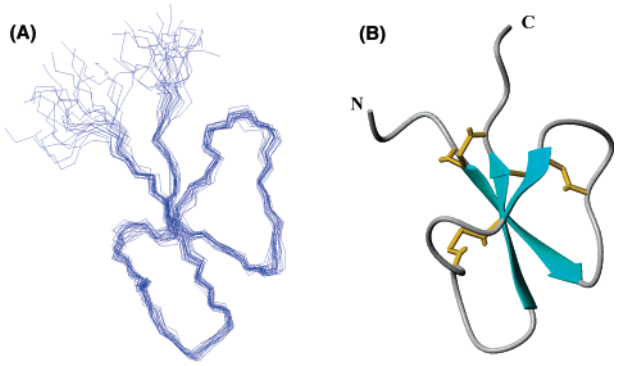

FIGURE 5: (A) Diagram of the backbone traces of the 20 lowest-energy structures of Crp4. (B) Ribbon diagram of the Crp4 structure with the three disulfide bonds colored gold. This figure was generated with MOLMOL.

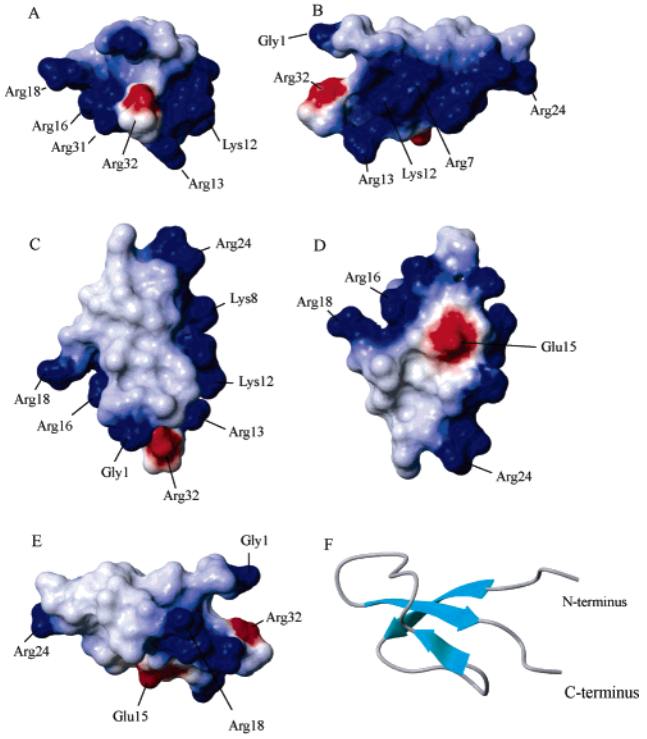

FIGURE 6: Charge distribution on the surface of Crp4. The basic regions of the protein are colored blue, whereas the acidic regions are colored red. This figure was produced with MOLMOL. Panels A−E show five different perspectives, while panel F shows the same view as panel E but in ribbon form. Arg32 is red because it is the carboxy-terminal residue in the protein.

residues forming a hydrophilic ring (Figure 6). As shown in Figure 6A−D, the arrangement of the hydrophobic and positive residues may perhaps better resemble two tightly fitting links of a chain with one link positive and the other hydrophobic in nature. The positive charges seem to be distributed about the perimeter in panels C and D of Figure 6, while the hydrophobic regions on two faces are joined around one side of the molecule (Figure 6E). This arrangement results in one region of charge-neutral residues, another region of positive residues, and a small isolated negative charge for Glu15. Given the anionic nature of the bacterial surface, the location of the positive charge around the periphery of the positive "link" of the chain may induce curvature of the bacterial membrane to permit maximum

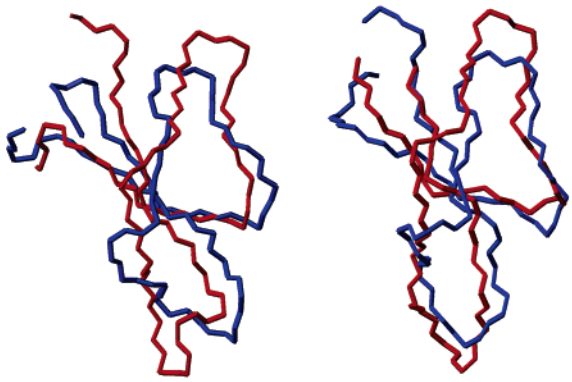

FIGURE 7: Overlay of the NMR structure of Crp4 (blue) with the NMR structure of RK-1 (left) and the crystal structure of HNP-3 (right).

electrostatic contact with Crp4. In this scenario, the hydrophobic regions of Crp4 would be drawn toward the hydrophobic inner membrane section. In this manner, membrane penetration could be achieved.

DISCUSSION

The aim of this study was to determine the three-dimensional solution structure of Crp4, a mouse Paneth cell α-defensin with potent and broad-range *in vitro* bactericidal activity. As expected, the structure of Crp4 indeed consists of a triple-stranded β-sheet, and these β-strands are connected by a series of tight turns and a β-hairpin.

So far, all the known mammalian defensins, irrespective of whether they are α- or β-defensins, adopt a similar overall structure, i.e., a triple-stranded antiparallel β-sheet. This structural feature may explain in part why defensins encoded by different genes and from various organisms differ in their antimicrobial spectrum and activity. Meanwhile, it is also implied that the triple-stranded β-sheet with its specific arrangement of disulfide bridges for defensins only confers a stability of their structures, but is not necessarily a determinant itself of antimicrobial activity. This is supported by a recent study showing that the disulfide bonding of HBD3 can be fully dispensed to its antimicrobial function but does influence HBD3 chemokine activity (*46*). Therefore, a comparison of the structures of different kinds of α-defensins should aid in a better understanding of the activities of these proteins.

Published coordinates for mammalian α-defensins deposited in the Protein Data Bank are limited to an X-ray study on HNP-3 (*47*), the NMR study on RK-1 (*45*), and the structural comparison between HNP-3 and RK-1 which has been performed previously (*45*). In Figure 7, the three-dimensional structure of Crp4 is superimposed with those of HNP-3 and RK-1. The Cα backbone of Crp4 and RK-1 can be overlayed with an rms distance of 3.37 Å, whereas the Cα rms distance of Crp4 with HNP-3 is 3.68 Å. The fairly poor overlay between these α-defensins results mainly from the following. First, the β-sheet content in these structures is different, with 34.4% in Crp4, 43.7% in RK-1, and 60% in HNP-3. The difference in β-sheet content between RK-1 and Crp4 is consistent with the data obtained from the D_2O exchange experiment. It was previously determined that 10 amide protons did not exchange 24 h after dissolution of RK-1 in D_2O (*45*), while only seven were

not exchanged in Crp4. The difference in exchange rates may also be interpreted as being part of a more flexible fold in the sheet structure which permits interaction of water with amide protons. The difference in homology between RK-1 and Crp4 may reflect the fold flexibility. Second, the length, shape, and orientation of the hairpin are different. As mentioned in the introductory section, Crp4 lacks three amino acids in the sequence between Cys^{IV} and Cys^{V}. However, the β-hairpin is unexpectedly longer than that of RK-1 and HNP-3 due to the relatively shorter β2 strand in Crp4. In addition, the hairpin in Crp4 is composed of two type I turns, while there are three turns comprising two type IV turns and one inverse γ-turn in RK-1, two turns in HNP-3, with one type IV and another type IV turn (*45*, *47*). There is currently no evidence concerning the relationship between the β-sheet content and the antimicrobial activity. However, the β-hairpin differences may be particularly interesting because of evidence that the β-hairpin loop is the active region of the rabbit neutrophil defensin NP-2 molecule (*48*). Possibly, the distinct hairpin structure in Crp4 contributes to its high *in vitro* potency, a hypothesis that can be tested directly by site-directed mutagenesis. Aside from the N- and C-termini, the β-hairpin loop of Crp4 may gain flexibility from the presence of two glycines found in the turn. The flexibility of the hairpin turn found in the hydrophobic portion of the peptide may account for an enhanced interaction with hydrophobic inner regions of bacterial membranes.

Another major difference between these α-defensins is the overall positive charge. Inspection of the Crp4 sequence indicates the presence of nine positively charged residues and only one negatively charged residue (Glu15), while RK-1 and HNP-3 possess one and two net positive charges, respectively. Significant net positive charges may be the most preserved characteristic of AMPs in general (*49*). This may explain the selective action of AMPs at negatively charged bacterial membranes. Most eukaryotic membranes, such as the plasma membrane of human erythrocytes, do not contain negatively charged lipids in the outer leaflet. Usually, increasing the overall positive charges will increase the microbicidal activity of AMPs. Indeed, Crp4 has been found to bind strongly to negatively charged model membranes, allowing Crp4 to associate more effectively with negatively charged biological membranes than neutral membranes (*50*).

Crp4 seems to require at least eight positive charges to maintain optimal bactericidal activity. Charge reversal mutagenesis at two positively charged positions diminishes *in vitro* antimicrobial activity markedly even though the net overall charge of the modified peptide remains positive (*25*). Also, the two proCrp4 processing intermediates ($proCrp4_{44-92}$ and $proCrp4_{54-92}$) possess the same number of positive charges as Crp4 and have the same bactericidal activity as the mature peptide (C. S. Weaks, H. Tanaka, and A. Y. Ouellette, unpublished observations). while full-length pro-Crp4 ($proCrp4_{20-92}$) has a net charge of 0 and lacks bactericidal activity (*50*). Our preliminary NMR results demonstrate that the isolated pro sequence of $proCrp4_{20-92}$ ($proCrp4_{20-60}$, containing eight negative charges) is very flexible and unstructured, suggesting that the anionic pro piece ($proCrp4_{20-60}$) might be able to neutralize the C-terminal mature cationic Crp4, thereby eliminating the antimicrobial activity of $proCrp4_{20-92}$. The task of determining the solution structure of intact $proCrp4_{20-92}$ is currently being pursued in our laboratory in an attempt to shed further light on this question.

It is also very interesting to note the sensitivity of the function of Crp4 to charge reversal. Any pair of site-directed Arg to Asp mutations in Crp4 attenuate or eliminate its microbicidal activity, regardless of the position of the Arg residue in the amino acid sequence (*25*). Compare this with the positive charge of +5 and negative charge of −4 for RK-1 to give an overall charge of +1 (Figure 1). Clearly, in the case of RK-1, having a significant portion of the molecule with a clear negatively charged character does not seem to impede the antimicrobial nature of the molecule.

Other studies have demonstrated that α-defensins act by permeabilizing the cell membranes of target microbes (*51*), but the details of the process are not yet clear. It has been proposed that the mode of α-defensins interacting with membranes is dependent on the conformation in solution. Dimeric human neutrophil defensins permeabilize model membranes by forming large, long-lived pores (*52*), while monomeric rabbit defensins disrupt membranes by causing a graded leakage (*53*). No evidence was found in the current NMR study that Crp4 is a dimer in solution, and indeed, it has been found that Crp4 induced graded leakage of fluorophores from phospholipid vesicles (*54*). However, Crp4 and rabbit neutrophil defensins have a high overall positive charge compared to RK-1, indicating that there is a difference in the mode of action between them, although they are all monomeric in solution. Therefore, extensive and direct comparisons of the membrane interactions of these peptides will be essential if a complete understanding of the mechanism of action of these AMPs is to be obtained.

ACKNOWLEDGMENT

We acknowledge the Canadian Foundation for Innovation (CFI), the Alberta Science and Research Authority, the Alberta Innovation Partnership program, and the AHFMR for the financial support in purchasing the 700 MHz NMR spectrometer and the cryoprobe for the 500 MHz instrument. The Bio-NMR facility is maintained through funds provided by CIHR and the University of Calgary. We are indebted to Dr. D. D. McIntyre for spectrometer upkeep.

REFERENCES

1. Ganz, T. (2003) Defensins: antimicrobial peptides of innate immunity, *Nat. Rev. Immunol. 3*, 710−720.
2. Schroder, J. M. (1999) Epithelial antimicrobial peptides: innate local host response elements, *Cell. Mol. Life Sci. 56*, 32−46.
3. Territo, M. C., Ganz, T., Selsted, M. E., and Lehrer, R. I. (1989) Monocyte-chemotactic activity of defensins from human neutrophils, *J. Clin. Invest. 84*, 2017−2020.
4. Chertov, O., Michiel, D. F., Xu, L., Wang, J. M., Tani, K., Murphy, W. J., Longo, D. L., Taub, D. D., and Oppenheim, J. J. (1996) Identification of defensin-1, defensin-2, and CAP37/azurocidin as T-cell chemoattractant proteins released from interleukin-8-stimulated neutrophils, *J. Biol. Chem. 271*, 2935−2940.
5. Yang, D., Chertov, O., Bykovskaia, S. N., Chen, Q., Buffo, M. J., Shogan, J., Anderson, M., Schroder, J. M., Wang, J. M., Howard, O. M., and Oppenheim, J. J. (1999) β-Defensins: linking innate and adaptive immunity through dendritic and T cell CCR6, *Science 286*, 525−528.
6. Ganz, T., Selsted, M. E., Szklarek, D., Harwig, S. S., Daher, K., Bainton, D. F., and Lehrer, R. I. (1985) Defensins. Natural peptide antibiotics of human neutrophils, *J. Clin. Invest. 76*, 1427−1435.
7. Jones, D. E., and Bevins, C. L. (1992) Paneth cells of the human small intestine express an antimicrobial peptide gene, *J. Biol. Chem. 267*, 23216−23225.

8. Bateman, A., MacLeod, R. J., Lembessis, P., Hu, J., Esch, F., and Solomon, S. (1996) The isolation and characterization of a novel corticostatin/defensin-like peptide from the kidney, *J. Biol. Chem. 271*, 10654−10659.
9. Wu, E. R., Daniel, R., and Bateman, A. (1998) RK-2: A novel rabbit kidney defensin and its implications for renal host defense, *Peptides 19*, 793−799.
10. Cole, A. M. (2003) Minidefensins and other antimicrobial peptides: Candidate anti-HIV microbicides, *Expert Opin. Ther. Targets 7*, 329−341.
11. Satoh, Y. (1988) Effect of live and heat-killed bacteria on the secretory activity of Paneth cells in germ-free mice, *Cell Tissue Res. 251*, 87−93.
12. Satoh, Y., Ishikawa, K., Ono, K., and Vollrath, L. (1986) Quantitative light microscopic observations on Paneth cells of germ-free and ex-germ-free Wistar rats, *Digestion 34*, 115−121.
13. Ayabe, T., Satchell, D. P., Wilson, C. L., Parks, W. C., Selsted, M. E., and Ouellette, A. J. (2000) Secretion of microbicidal α-defensins by intestinal Paneth cells in response to bacteria, *Nat. Immunol. 1*, 113−118.
14. Porter, E. M., Bevins, C. L., Ghosh, D., and Ganz, T. (2002) The multifaceted Paneth cell, *Cell. Mol. Life Sci. 59*, 156−170.
15. Geyer, G. (1973) Lysozyme in Paneth cell secretions, *Acta Histochem. 45*, 126−132.
16. Peeters, T., and Vantrappen, G. (1975) The Paneth cell: A source of intestinal lysozyme, *Gut 16*, 553−558.
17. Short, M. L., Nickel, J., Schmitz, A., and Renkawitz, R. (1996) Lysozyme gene expression and regulation, *EXS 75*, 243−257.
18. Nyman, K. M., Ojala, P., Laine, V. J., and Nevalainen, T. J. (2000) Distribution of group II phospholipase A2 protein and mRNA in rat tissues, *J. Histochem. Cytochem. 48*, 1469−1478.
19. Hooper, L. V., Stappenbeck, T. S., Hong, C. V., and Gordon, J. I. (2003) Angiogenins: A new class of microbicidal proteins involved in innate immunity, *Nat. Immunol. 4*, 269−273.
20. Bevins, C. L., Martin-Porter, E., and Ganz, T. (1999) Defensins and innate host defence of the gastrointestinal tract, *Gut 45*, 911−915.
21. Ouellette, A. J., and Selsted, M. E. (1996) Paneth cell defensins: Endogenous peptide components of intestinal host defense, *FASEB J. 10*, 1280−1289.
22. Ouellette, A. J., and Bevins, C. L. (2001) Paneth cell defensins and innate immunity of the small bowel, *Inflamm. Bowel Dis. 7*, 43−50.
23. Ouellette, A. J., Hsieh, M. M., Nosek, M. T., Cano-Gauci, D. F., Huttner, K. M., Buick, R. N., and Selsted, M. E. (1994) Mouse Paneth cell defensins: Primary structures and antibacterial activities of numerous cryptdin isoforms, *Infect. Immun. 62*, 5040−5047.
24. White, S. H., Wimley, W. C., and Selsted, M. E. (1995) Structure, function, and membrane integration of defensins, *Curr. Opin. Struct. Biol. 5*, 521−527.
25. Tanabe, H., Qu, X., Cummings, J. E., Kolusheva, S., Weeks, C. S., Walsh, K. B., Jelinek, B., Vanderlick, T. K., Selsted, M. E., and Ouellette, A. J. (2004) Structure−activity determinants in paneth cell α-defensins: Loss-of-function in mouse cryptdin-4 by charge-reversal at arginine residue positions, *J. Biol. Chem. 279*, 11976−11983.
26. Shirafuji, Y., Tanabe, H., Satchell, D. P., Henschen-Edman, A., Wilson, C. L., and Ouellette, A. J. (2003) Structural determinants of procryptdin recognition and cleavage by matrix metalloproteinase-7, *J. Biol. Chem. 278*, 7910−7919.
27. Braunschweiller, L., and Ernst, R. R. (1983) Coherence Transfer by Isotropic Mixing: Application to Proton Correlation Spectroscopy, *J. Magn. Reson. 53*, 521−528.
28. Jeener, J., Meier, B. H., Bachmann, L., and Ernst, R. R. (1979) Investigation of exchange processes by two-dimensional NMR spectroscopy, *J. Chem. Phys. 71*, 4546−4553.
29. Rance, M., Sorenson, O. W., Bodenhausen, G., Wagner, G., Ernst, R. R., and Wuthrich, K. (1983) Improved spectral resolution in cosy ^{1}H NMR spectra of proteins via double quantum filtering, *Biochem. Biophys. Res. Commun. 117*, 479−485.
30. Callihan, D., West, J., Kumar, S., Schweitzer, B. I., and Logan, T. M. (1996) Simple, distortion-free homonuclear spectra of peptides and nucleic acids in water using excitation sculpting, *J. Magn. Reson. 112*, 82−85.
31. Delaglio, F., Grzesiek, S., Vuister, G. W., Zhu, G., Pfeifer, J., and Bax, A. (1995) NMRPipe: A multidimensional spectral processing system based on UNIX pipes, *J. Biomol. NMR 6*, 277−293.
32. Johnson, B. A., and Blevins, R. A. (1994) NMRView: A computer program for the visualization and analysis of NMR data, *J. Biomol. NMR 4*, 603−614.
33. Jones, J. A., Wilkins, D. K., Smith, L. J., and Dobson, C. M. (1997) Characterization of protein unfolding by NMR diffusion experiments, *J. Biomol. NMR 10*, 199−203.
34. Merrill, M. R. (1993) NMR diffusion measurements using a composite gradient PGSE sequence, *J. Magn. Reson. 103*, 223−225.
35. Gibbs, S. J., and Johnson, C. S., Jr. (1991) A PFG NMR experiment for accurate diffusion and flow studies in the presence of Eddy currents, *J. Magn. Reson. 93*, 395−402.
36. Wüthrich, K. (1986) *NMR of Proteins and Nucleic Acids*, pp 130−161, John Wiley and Sons, New York.
37. Nilges, M. (1995) Calculation of protein structures with ambiguous distance restraints. Automated assignment of ambiguous NOE crosspeaks and disulphide connectivities, *J. Mol. Biol. 245*, 645−660.
38. Koradi, R., Billeter, M., and Wüthrich, K. (1996) MOLMOL: A program for display and analysis of macromolecular structures, *J. Mol. Graphics 14*, 51−55.
39. Nicholls, A., Sharp, K. A., and Honig, B. (1991) Protein folding and association: Insights from the interfacial and thermodynamic properties of hydrocarbons, *Proteins 11*, 281−296.
40. Wilkins, D. K., Grimshaw, S. B., Receveur, V., Dobson, C. M., Jones, J. A., and Smith, L. J. (1999) Hydrodynamic radii of native and denatured proteins measured by pulse field gradient NMR techniques, *Biochemistry 38*, 16424−16431.
41. Schibli, D. J., Hunter, H. N., Aseyev, V., Starner, T. D., Wiencek, J. M., McCray, P. B., Jr., Tack, B. F., and Vogel, H. J. (2002) The solution structures of the human β-defensins lead to a better understanding of the potent bactericidal activity of HBD3 against *Staphylococcus aureus*, *J. Biol. Chem. 277*, 8279−8289.
42. Hunter, H. N., Fulton, D. B., Ganz, T., and Vogel, H. J. (2002) The solution structure of human hepcidin, a peptide hormone with antimicrobial activity that is involved in iron uptake and hereditary hemochromatosis, *J. Biol. Chem. 277*, 37597−37603.
43. Weljie, A. M., Yamniuk, A. P., Yoshino, H., and Vogel, H. J. (2003) Protein conformational changes studied by diffusion NMR spectroscopy: Application to helix-loop-helix calcium binding proteins, *Protein Sci. 12*, 228−236.
44. Wishart, D. S., Sykes, B. D., and Richards, F. M. (1992) The chemical shift index: A fast and simple method for the assignment of protein secondary structure through NMR spectroscopy, *Biochemistry 31*, 1647−1651.
45. McManus, A. M., Dawson, N. F., Wade, J. D., Carrington, L. E., Winzor, D. J., and Craik, D. J. (2000) Three-dimensional structure of RK-1: A novel α-defensin peptide, *Biochemistry 39*, 15757−15764.
46. Wu, Z., Hoover, D. M., Yang, D., Boulegue, C., Santamaria, F., Oppenheim, J. J., Lubkowski, J., and Lu, W. (2003) Engineering disulfide bridges to dissect antimicrobial and chemotactic activities of human β-defensin 3, *Proc. Natl. Acad. Sci. U.S.A. 100*, 8880−8885.
47. Hill, C. P., Yee, J., Selsted, M. E., and Eisenberg, D. (1991) Crystal structure of defensin HNP-3, an amphiphilic dimer: Mechanisms of membrane permeabilization, *Science 251*, 1481−1485.
48. Thennarasu, S., and Nagaraj, R. (1999) Synthetic peptides corresponding to the β-hairpin loop of rabbit defensin NP-2 show antimicrobial activity, *Biochem. Biophys. Res. Commun. 254*, 281−283.
49. Epand, R. M., and Vogel, H. J. (1999) Diversity of antimicrobial peptides and their mechanisms of action, *Biochim. Biophys. Acta 1462*, 11−28.
50. Satchell, D. P., Sheynis, T., Shirafuji, Y., Kolusheva, S., Ouellette, A. J., and Jelinek, R. (2003) Interactions of mouse Paneth cell α-defensins and α-defensin precursors with membranes. Prosegment inhibition of peptide association with biomimetic membranes, *J. Biol. Chem. 278*, 13838−13846.
51. Lehrer, R. I., Szklarek, D., Ganz, T., and Selsted, M. E. (1985) Correlation of binding of rabbit granulocyte peptides to *Candida albicans* with candidacidal activity, *Infect. Immun. 49*, 207−211.
52. Wimley, W. C., Selsted, M. E., and White, S. H. (1994) Interactions between human defensins and lipid bilayers: Evidence for formation of multimeric pores, *Protein Sci. 3*, 1362−1373.
53. Hristova, K., Selsted, M. E., and White, S. H. (1996) Interactions of monomeric rabbit neutrophil defensins with bilayers: Com-

parison with dimeric human defensin HNP-2, *Biochemistry 35*, 11888−11894.
54. Satchell, D. P., Sheynis, T., Kolusheva, S., Cummings, J., Vanderlick, T., Jelinek, R., Selsted, M. E., and Ouellette, A. J. (2003) Quantitative interactions between cryptdin-4 amino terminal variants and membranes, *Peptides 24*, 1795−1805.
55. Laskowski, R. A., Rullmann, J. A. C., MacArthur, M. W., Kaptein, R., and Thornton, J. M. (1996) AQUA and PROCHECK-NMR: Programs for checking the quality of protein structures solved by NMR, *J. Biomol. NMR 8*, 477−486.

BI048645P